Rare Metal Materials and Engineering
Volume 47, Issue 10, October 2018
Online English edition of the Chinese language journal

Available online at www.sciencedirect.com
ScienceDirect

Cite this article as: Rare Metal Materials and Engineering, 2018, 47(10): 2986-2992.

ARTICLE

Preparation and Properties of a New Cost-effective Amorphous Composite Coating

Shang Junchao[1], Liang Xiubing[2], Chen Yongxiong[2], Xu Binshi[1], Cao Wei[3]

[1] National Defense Key Laboratory for Remanufacturing Technology, Army Academy of Armored Forces, Beijing 100072, China; [2] National Innovation Institute of Defense Technology, Academy of Military Science PLA China, Beijing 100070, China; [3] 63963 PLA Troops, Beijing 100072, China

Abstract: A NiFeBSiNb amorphous/nanocrystalline composite coating was prepared through flame thermal spraying, where a gas atomized alloy powder substituted an amorphous powder. The microstructure and thermal behavior of the laboratory-produced powders and the produced as-sprayed coating were characterized. The results demonstrate that the powder, which is spherical or ellipsoidal, is mainly composed of $Nb_2Ni_{21}B_6$ and $(Ni,Fe)_{23}B_6$ crystalline phases, whereas the as-sprayed coating consists of a glassy structure and certain nanocrystalline phases. It is obtained through calculations that the R_c (critical cooling rate) of the powder and the as-sprayed coating for the amorphous phase formations is 6.01×10^5 and 4.56×10^3 K/s, respectively. The explanation for the amorphous structure, as it occurred in the as-sprayed coating, is the rapid quenching from the melt at the cooling rates which exceeds the critical cooling rate R_c. The as-sprayed amorphous coatings displays a low friction coefficient of 0.17 and excellent wear resistance.

Key words: amorphous coating; alloy powder; flame spraying; wear

The metallic glass, or amorphous alloy, is one of the most promising engineering materials which demonstrates high hardness, high strength, superior wear and corrosion resistance[1-3]. In contrast, the low three-dimensional size property, the high cost and the low toughness have restricted the corresponding applications in industry; however, the application of coatings as an alternative has proven to be an improved method to exploit attributes, such as wear and corrosion resistances[4-6]. Amorphous metallic coatings can be synthesized through thermal spraying, such as melting and rapid cooling of alloy powder feedstocks, which have the high potential for the synthesis of amorphous/nanocrystalline coatings through the rapid cooling rate. The solidification process is possible for the amorphous phase to form, owing to the suppressed long-range order of the arranged atoms and the nucleation and growth of the crystalline phases. During the last few decades, a large number of reports regarding thermal spray techniques were known, such as flame spray, plasma spray, high velocity oxygen fuel spray and cold spray. They were applied to the fabrication of amorphous metallic coatings[7-12]. Currently, a growing interest exists in Ni-based amorphous coatings, which exhibit high toughness, excellent thermal stability and good corrosion resistance. Sampath[13] reported that Ni-Mo based metallic glass coatings (MGCs) can be obtained through vacuum plasma spraying (VPS) and air plasma spraying (APS). Wang et al[14] observed that the Ni-Zr-Ti-Si-Sn partial amorphous coating, equaling the amorphous ribbon in wear and corrosion resistance, was fabricated through a high velocity air fuel (HVAF) thermal spraying process. Li et al[15] reported that the structure and corrosion resistance properties of Ni-Fe-B-Si-Nb amorphous/ nanocrystalline composite coating were produced through laser processing. In contrast, researchers have concentrated the corresponding attention on the utilization of amorphous powders to obtain amorphous coatings, and have rarely studied the high potentials of alloy powder in the amorphous

Received date: November 10, 2017
Foundation item: National Natural Science Foundation of China (51375492, 51575527)
Corresponding author: Liang Xiubing, Ph. D., Professor, National Innovation Institute of Defense Technology, Academy of Military Science PLA China, Beijing 100070, P. R. China, Tel: 0086-10-66717351, E-mail: liangxb_d@163.com

coatings fabrication. Consequently, relevant researches are confined to the experimental properties in the laboratory, instead of being applied to industries.

It is well known that there are two significant factors affecting amorphous coatings: one is the high glass forming ability of the original material and the wide supercooled liquid region, whereas the other is the rapid quenching from the melt to restrain the nucleation and growth of the crystalline phase during spraying[16]. It is consequently possible to use economical alloy powders with high glass forming ability to substitute the costly amorphous powders in the syntheses of amorphous coatings. Until recently, Ni-based bulk glass formation with high glass forming ability was achieved such as Ni-Nb-Ti-Zr, Ni-Nb-Zr-Ti-(Pt,Cu), Ni-Ti-Zr-Si-Sn, Ni-Zr-Nb-Al, Ni-Pd-P-(B,Si) and Ni-Cu-Ti-Zr-Al rods with millimeter in diameter[17-23], whereas these alloys containing titanium and zirconium are not recommended for air rich thermal spraying, due to the corresponding susceptibility to oxidation and uneconomical price. In contrast, the $[(Ni_{0.6}Fe_{0.4})_{0.75}B_{0.2}Si_{0.05}]_{96}Nb_4$ [24,25] in the composite alloy with a high glass forming ability exhibits a super high fracture strength of 3800 MPa and good corrosion resistance. Moreover, the boron element in the alloys will prefer to combine with oxygen, which prevents the oxidation of other elements due to oxide evaporation.

In the present study, a new type of Ni-Fe-B-Si-Nb composite alloy with high glass forming ability was designed for thermal spraying, from which the amorphous and nanocrystalline composite coating was obtained through flame spraying. A laboratory prepared crystal powder by gas atomization was used as the spraying feedstock to replace amorphous powders. This was, by far, a hardly-treated way in the preparation of an amorphous coating, to save costs and extend the applications in industry.

1 Experiment

A $Ni_{60}Fe_{16}B_{17}Si_3Nb_4$ alloy ingot was prepared through induction-melting of industrial alloys such as ferro-boron, ferro-silicon, ferro-niobium and pure nickel balance in a zirconia crucible under an argon atmosphere. The $Ni_{60}Fe_{16}B_{17}Si_3Nb_4$ crystal powder was produced through argon atomization at a pressure of 0.65~7.0 MPa, followed by superheating at 200~250 °C. Consequently, the powder was collected, sieved and divided into different size ranges. The flame CP-3000 thermal spraying equipment was used to fabricate the coating onto 0.45% carbon steel. The parameters are presented in Table 1.

The phase analysis of the coating and powder was performed with a D8 X-ray diffractometer (XRD) of a Cu Kα X-ray source with an incidence beam angle of 2°. The diffraction scanning angles ranged between 20°~100° at a scanning rate of 0.02°/s. The microstructures of the powder, the coating cross section and the coating wear surface were characterized through a Nova nano field emission microstructure scanning electron microscope 650 (SEM) with an accelerating voltage of 20 kV, which was equipped with an energy dispersive spe trometer (EDS). Also, a Tecnai F30 transmission electron microscope was employed. The thermal stability of the crystal powders and the coating was examined with a differential scanning calorimeter in a continuous heating mode, at a rate of 10 K/min. The friction and wear properties of the coatings were evaluated using an UMT-3 multifunction friction and wear tester. The counter body was made of GCr15 steel.

Table 1 Flame thermal spraying parameters of NiFeBSiNb amorphous coating

Parameter	Value
Fuel(C_2H_2) pressure/MPa	0.13
Fuel flow/$m^3 \cdot h^{-1}$	1.3
O_2 pressure/MPa	0.7
O_2 flow/$m^3 \cdot h^{-1}$	1.25
Powder feeding rate/$g \cdot min^{-1}$	35
Spraying distance/mm	180
Cooling gas pressure/MPa	0.4

2 Results and Discussion

2.1 Powder and coating structure

Fig.1 presents the XRD patterns of the NiFeBSiNb atomized crystal powder and the as-deposited coating. The powder structure mainly consists of crystalline phases that are identified as $Nb_2Ni_{21}B_6$ and $(Ni,Fe)_{23}B_6$, whereas almost no amorphous phases exist in the powder. However, the as-deposited coating has a broad halo peak at the 2θ=40°~50°, whereas the diffraction peaks of the coating become apparently lower. It is indicated that certain amorphous phases coexist with the crystalline phases.

It is basically confirmed that the Ni-based composite coating can be fabricated through flame spraying crystal alloy powders. Undoubtedly, the material composition is primary in all factors affecting the amorphous coating preparation. The composition of the presented NiFeBSiNb alloy belongs to three empirical rules[26]: (1) multicomponent systems, consisting of more than three elements; (2) a significant differences in atomic size ratios (exceeding 12% approximately) among the three main constituent elements; and (3) negative mixing heats among the three main constituent elements. The designed powder is composed of five types of elements, including the early transition metal (ETM) Nb, the late transition metal (LTM) Fe, Ni and the metalloids B and Si. The atomic radii of Nb, Fe, Ni, Si and B are 0.208, 0.172, 0.162, 0.146 and 0.117 nm, respectively. The atomic sizes of the elements decrease in the following order: Nb＞Fe＞Ni＞Si＞B. The main atomic pairs have a high negative mixing enthalpy, where the mixing enthalpies of Nb-Ni, Nb-Fe, Nb-B and Nb-Si are –16, –30, –54 and –56 kJ/mol, respectively[27], which is attributed to the high glass forming ability of the

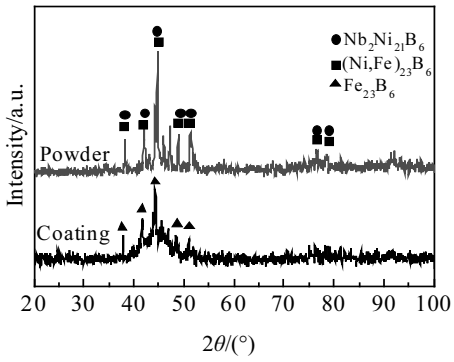

Fig.1 XRD patterns of NiFeBSiNb powder and as-deposited coating

alloy system, the forming of highly dense random packed atomic configurations and the lower atomic diffusivity. When the material system is determined, the melting becomes particularly significant, affecting the amorphous formation. Mcvahedi[28] reported that through a high velocity oxygen fuel process (HVOF) fuel/oxygen ratios adjustment, a fully amorphous coating could be obtained with the increase the flame temperature. Otherwise, the crystalline phase would emerge and increase in size. Wang[14] could not obtain the fully amorphous coatings of Ni-based materials through the high velocity air fuel (AC-HVAF) spraying process activation, which had higher spraying particle velocity and lower flame temperature than the HVOF process. It is suggested that when the flame temperature exceeds the amorphous powders crystallization temperature or the melting temperature of the amorphous powders is lowered, the crystalline phase content in the coating increases. The present flame spraying has a high flame temperature (~3500 °C) and a low spraying particle velocity. In this case, the particles could stay in the flame longer and melt completely. This is advantageous for the amorphous coating formation. The high cooling rate is certainly necessary to quench the molten liquid droplets for the amorphous phases to form. Therefore, although the powder of the atomized gas in the present study consists of almost crystalline phases, the amorphous phases could be finally produced in the coating. This means that the cooling rate of the fabricated powder is lower than the critical cooling rate of the amorphous phase formation, while it exceeds the critical value during spraying.

2.2 Microstructural observations

Fig.2a presents the SEM image of the atomized powders. Most particles are near-spherical or spherical, ensuring a good flow for the flame spraying. Rough dendrite structures and pores caused by the gas evolution in the large-sized particles exist along with certain attached satellite particles, whereas the small-sized particle surfaces are smooth and certain satellite particles are attached. The metal droplet diameter R changes, following the droplet cooling rate, and it can be expressed as[29]:

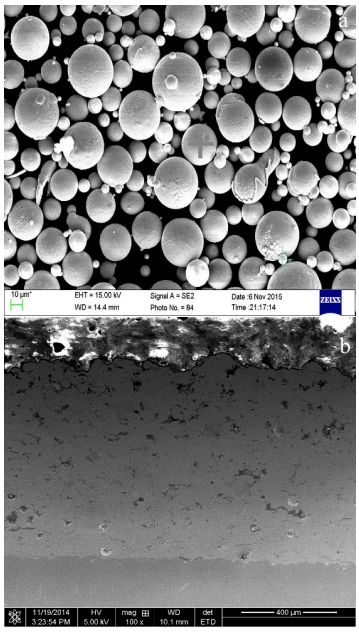

Fig.2 SEM image of atomized powders (a) and cross-section of amorphous coating (b)

$$R=\frac{\mathrm{d}T_{\mathrm{d}}}{\mathrm{d}t}=\frac{C}{d} \tag{1}$$

$$C=\frac{6}{C_1\rho_{\mathrm{d}}}\left[h\left(T_{\mathrm{gas}}-T_{\mathrm{d}}\right)+\varepsilon\delta\left(T_{\mathrm{W}}^4-T_{\mathrm{d}}^4\right)\right] \tag{2}$$

where, C_1 is the specific heat capacity of the liquid droplet material (J/kg·K), ρ_{d} is the droplet density (g/m^3), h is the heat transfer coefficient, T_{gas} is the gas temperature, T_{d} is the droplet temperature, ε and δ are the emissivity and Stefan-Boltzmann constant, respectively, and T_{w} is the temperature of the surrounding walls. The droplet speed is almost unchanged in a significantly short period of time, C could be viewed as a constant, the heat transfer coefficient h is only inversely proportional to the droplet diameter R. Therefore, the higher the cooling rate is, the smaller the diameter of the obtained droplets is. Different diameters of droplets represent different microstructures, such as the planar, the cellular, the dendritic and the cell planar shapes with the increase of cooling rate[30]. This is the reason for the large particle surface being mostly a dendrite structure and the small-sized particle surface being a smooth cellular structure. Fig.2b presents the cross-sectional image of the amorphous coating prepared through flame spraying. It exhibits that the coating is compact and dense. The particles melt fully having a significantly good connection each other. The coating adher well to the substrate without cracking. Certain pores could be observed in the coating microstructure. The large-sized pores around impurities are mainly caused by the loose lapping of the particle deposition. The smell-sized pores are formed from the cracking by the molten particle rapid quenching. Through

comparison, porosity existing at the bottom of the coating is smaller than that at the top. During spraying, the deposition of molten droplets releases the latent heat in solidification, and softens the deposited particles through increasing the temperature to the near glass transition temperature of the amorphous alloys[31]. This leads to the plastic deformation of the plats becoming highly dense. Table 2 presents the EDS results of the Ni-based crystal powder and the amorphous coating. The composition of the coating is basically in agreement with that of the powder. Oxides are inevitably generated in the coating, whereas the O levels is 1.88 wt%.

Fig.3 presents the TEM images and the corresponding selected area diffraction patterns (SADP) of the NiFeBSiNb coating. It could be confirmed that there is a fully amorphous structure in the as-sprayed coating which is expected from a wide range of features, as observed in Fig.3a. The as-sprayed coating essentially consists of amorphous phases, except for individual regions, which consists of the amorphous phase and nanocrystalline grains, as presented in Fig.3b and 3c. Fig.3b presents that a mixture of nanocrystalline grains of 20~50 nm is distributed within the amorphous matrix. The electron diffraction pattern also exhibits a diffused amorphous halo, in which diffraction spots occur from the nanocrystalline grains. In contrast, certain nanocrystalline grains become coarser to approximately 200~300 nm, as presented in Fig.3c. These grains mainly include boride, which is calibrated to the $Fe_{23}B_6$ [$\bar{1}$11] crystal axis. The TEM image of the as-sprayed coating confirms that the amorphous/nanocrystalline structure could be fabricated from the crystal powder. The rapid quenching of the fully melt particles at a sufficiently fast cooling rate could suppress the nucleation and achieve amorphization. It should be noted that certain crystal grains are unavoidable, due to the excessive partial melting of the particles, as well as the subsequent impact and heat transfer of the particles.

2.3 Thermal behavior

Fig.4 presents the DSC curve of the as-sprayed NiFeBSiNb amorphous coating. The sample exhibits two exothermic peaks, due to the glass transition. The glass transition temperature T_g, the onset temperature of the first crystallization event T_x, the melting (T_m) and the liquidus (T_l) temperature are marked with arrows in Fig.4. The supercooled liquid region ΔT_x ($\Delta T_x=T_x-T_g$) and the reduced glass transition temperature T_{rg} ($T_{rg}=T_g/T_l$) (Table 3) are in accordance with the findings of other researchers[25]. The criterion for the glass-forming ability (GFA) γ and the critical cooling rate R_c can be evaluated as[32]:

$$\gamma = T_x/(T_g + T_l) \quad (3)$$

$$R_c = 5.1\times10^{21}\exp(-117.19\gamma) \quad (4)$$

The results demonstrate that the criterion for GFA is γ=0.348 and the critical cooling rate is R_c=4.56×10^3 K/s. Consequently, considering that the cooling rate of flame spraying could exceed 10^5 K/s, the fully molten alloy powder could form a

Table 2 EDS results of NiFeBSiNb powder and amorphous coating (wt%)

Material	Ni	Fe	Si	Nb	B	O
Powder	69.9	16.3	4.52	4.90	4.38	
Coating	67.64	17.51	5.19	4.80	2.98	1.88

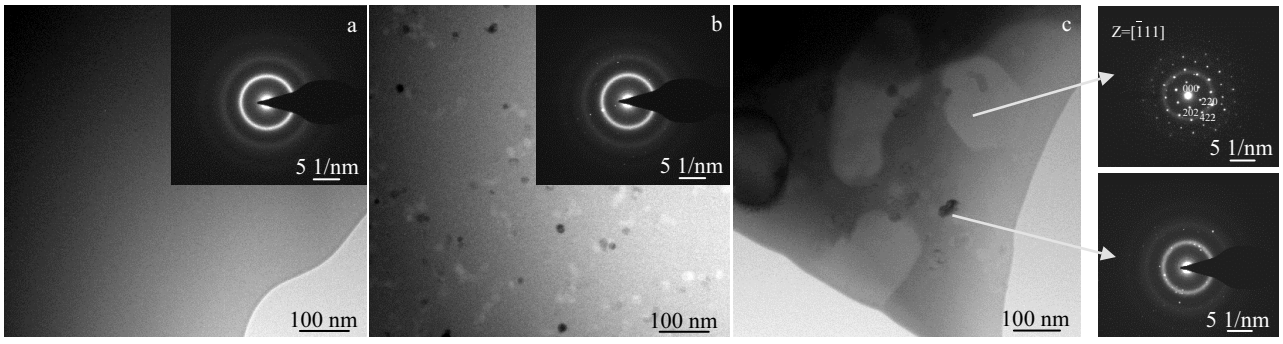

Fig.3 TEM bright field images and corresponding SADP of NiFeBSiNb coating: (a) fully amorphous phase; (b) amorphous/nanocrystallization phase; (c) crystallization phase

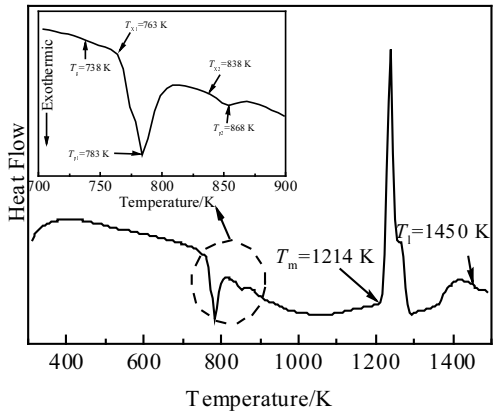

Fig.4 DSC curve of as-sprayed NiFeBSiNb amorphous coating

Table 3 Thermal parameters of as-sprayed NiFeBSiNb amorphous coating

T_{g1}/K	T_{x1}/K	T_{p1}/K	ΔT_x/K	T_{x2}/K	T_{p2}/K	T_m/K	T_l/K	T_{rg}
738	763	783	25	838	868	1214	1450	0.57

completely amorphous phases through rapidly quenching. In contrast, in the gas atomization of the powder, the melt of the alloy retains the superheating of approximately 250 K, in order to melt the insoluble crystal phase and the droplet pass smoothly through the diversion tube. The γ and R_c of the powder are evaluated as 0.312 and 6.01×10^5 K/s, respectively. This is the reason for the amorphous powder formation being quite difficult compared to the as-sprayed coating.

Fig.5 is the schematic time-temperature-transformation (TTT) diagram for the onset of crystallization of a glass-forming liquid[33]. The onset of crystallization always occurs easily in the nose of the TTT curve between T_l and T_g. This temperature is expressed as $T_n=a(T_l+T_n)$ and the parameter a is between 0.45 and 0.55. In order to avoid the crystallization, the liquid must be quenched with the cooling rate $R\geq R_c$ (R_c, the critical cooling rate to form a glass, can be defined as $R_c=(T_l-T_n)/t_n$). The NiFeBSiNb amorphous alloy R_c value is roughly estimated to be 1.15×10^3 K/s, according to Ref. [25], which is consistent with the R_c result of the coating. In the flame spraying process, the melt of Ni-based alloy particles could be deposited and solidified on the substrate, passing a distance of 200 mm at a speed of 100 m/s, and its temperature drops from 1400 K to 400 K, simultaneously. The cooling rate of the particles can be evaluated to be 5×10^5 K/s, which is far beyond R_c. Therefore, the Ni-based alloy particles deposited on the substrate can form an amorphous phase in the flame spraying process.

2.4 Coating friction and wear properties

Fig.6 presents the microhardness distribution from the substrate to the coating surface. The coating hardness is undulated in a narrow range of 6.5~8.5 GPa. This contributed to the uniform and dense structure of the coating. The average hardness value of the coating is approximately 7 GPa, which is higher than that of the alloy with the same composition due to the numerous amorphous phases, nanocrystalline phases and borides in the coating. Fig.7 presents the friction coefficients of the coating and the substrate under the experimental conditions of 5 N, 5 Hz, 30 min and dual GCr15. The friction coefficient of the substrate is approximately 0.4. Within 0~500 s, the friction coefficient increases and tends to stabilize at approximately 0.4 at 700 s, following a narrow range of fluctuations. The friction coefficient of the coating is approximately 0.17. Within 0~300 s, the friction coefficient of the coating demonstrates a high fluctuation and an apparent running at this stage. Consequently, it tends to be flat after 300 s, about 0.17. The coating with the low friction coefficient is attributed to the amorphous phase without grain boundaries, dislocations and lattice distortion. The grain boundary is one of the micro factors affecting the material friction properties. During sliding, the near surface dislocation of the friction contact, which is accumulated, could be blocked by the grain boundary. This induces strain hardening on the friction surface; as a result, the dislocation movement becomes significantly difficult to increase the material friction force.

Fig.8 presents the worn surfaces of the as-sprayed coating and the substrate. The worn surface of the composite coating

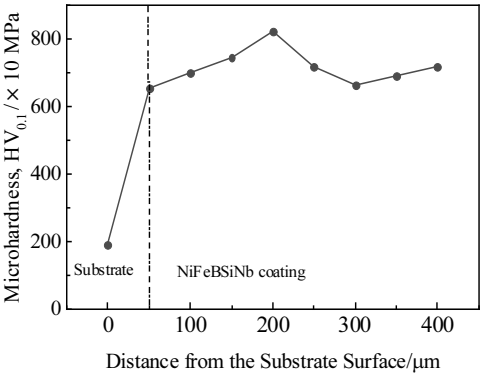

Fig.6 Coating microhardness

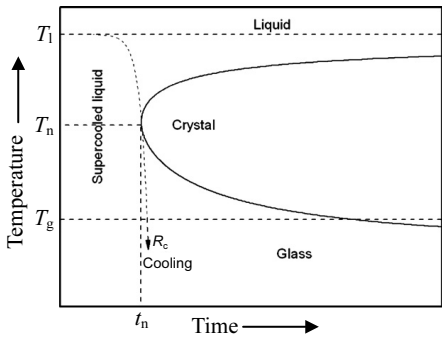

Fig.5 Schematic time-temperature-transformation (TTT) diagram for the onset of crystallization of a glass-forming liquid[33]

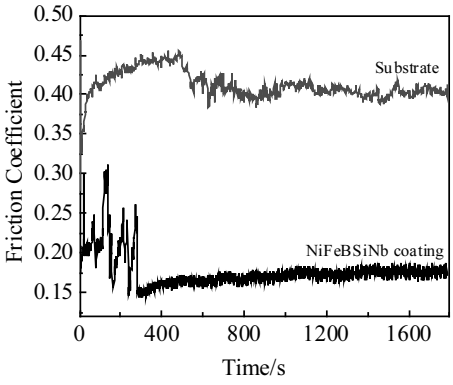

Fig.7 Comparison of friction coefficients between coating and substrate

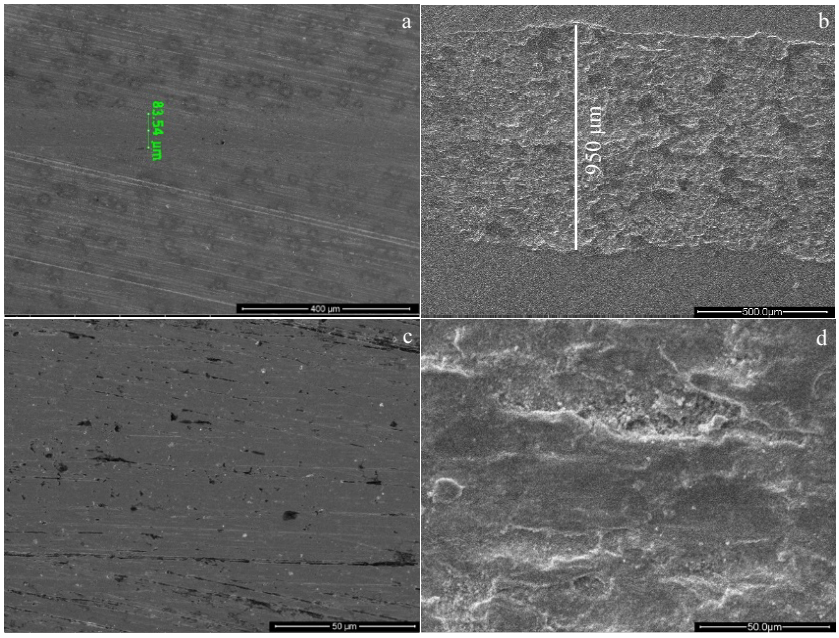

Fig.8 Wear track of coating and 0.45% carbon steel substrate: (a) wear track of coating; (b) wear track of substrate; (c) under high multiple wear passes of coating; (d) under high multiple wear passes of substrate

is smooth and shallow (Fig.8a). Certain slight furrows exist along the sliding direction. This is contributed to the abrasive particles, such as boron compound hard phases, to peel off the coating while the worn surface is cut and plowed, suggesting that abrasion is the main wear mechanism. The abrasion width of the coating is only 83.54 μm, which is 10 times lower than 950 μm of the 0.45% carbon steel substrate. Fig.8b presents the worn surface of the substrate. It is visible that numerous detached areas exist on the worn surface of the substrate which sustains a plastic deformation, indicating that adhesion is the dominant wear mechanism.

The amorphous coating exhibits sufficiently good wear resistance compared to the substrate. Firstly, the coating has a significantly higher hardness than that of the substrate. Furthermore, many flaws, such as dislocations and grain boundary movements, do not exist in the amorphous structure. Therefore, its friction coefficient is low. Only a small amount of boride and oxide exist, which are brittle and prone to flaking off from the boundary of the tabular droplets to be embedded into the worn surface, causing abrasive wear. In contrast, for the crystalline materials, the grain boundaries could inhibit the dislocation surface movement and lead to a continuous accumulation, causing strain hardening of the surface and increasing friction of the contact surfaces. Consequently, the substrate displays a high friction coefficient, severe plastic deformation and adhesivewear.

3 Conclusions

1) The gas atomized near-spherical or spherical powders mainly consist of $Nb_2Ni_{21}B_6$ and $(Ni,Fe)_{23}B_6$ crystal phases.

2) The amorphous/nanocrystalline coating can be fabricated through flame thermal spraying using the crystalline alloy powder as the feedstock. The microstructure of the as-sprayed coating consists of completely amorphous, nanocrystalline and $Fe_{23}B_6$ crystal phases.

3) The reason for the emergence of the amorphous structure in the as-sprayed coating is the rapid quenching from the melt, at a cooling rate which exceeds the critical cooling rate R_c of 4.56×10^3 K/s. The as-sprayed amorphous coatings have a low friction coefficient of 0.17 and excellent wear resistance.

References

1 Inoue A, Takeuchi A. *Acta Materialia*[J], 2011, 59 (16): 2243
2 Inoue A, Baolong S, Takeuchi A. *Materials Transactions*[J], 2006, 47(5): 1275
3 Eugen Axinte. *Materials and Design*[J], 2012, 35: 518
4 Guo Wenmin, Wu Yuping, Zhang Jianfeng *et al*. *Journal of Thermal Sprayed Technology*[J], 2014, 23(7): 1157
5 Wang A P, Wang Z M, Zhang J *et al*. *Journal of Alloys and Compounds*[J], 2007, 440: 225
6 Wang Gang, Huang Zhongjia, Xiao Ping *et al*. *Journal of Manufacturing Processes*[J], 2016, 22: 34
7 Voyer J. *Journal of Thermal Spray Technology*[J], 2010, 19(5): 1013
8 Suresh K, Yugeswaran S, Rao K P *et al*. *Vacuum*[J], 2013, 88: 114
9 Kumar S, Kim Junseoub, Kim Hwijun *et al*. *Journal of Alloys and Compounds*[J], 2009, 475: 9

10 Jayaraj J, Sordelet D J, Kim D H *et al*. *Corrosion Science*[J], 2006, 48: 950
11 Zhou Z, Wang L, He D Y *et al*. *Journal of Thermal Spray Technology*[J], 2010, 19(6): 1287
12 Henao John, Concustell Amadeu, Irene G *et al*. *Materials and Design*[J], 2016, 94: 253
13 Sampath S. *Materials Science and Engineering A*[J], 1993, 167: 1
14 Wang Aiping, Zhang Tao, Wang Jianqiang. *Materials Transactions*[J], 2005, 46(5): 1010
15 Li Ruifeng, Li Zhuguo, Zhu Yanyan *et al*. *Journal of Alloys and Compounds*[J], 2013, 580: 327
16 Zois D, Lekatou A, Vardavoulias M. *Journal of Alloys and Compounds*[J], 2010, 495(2): 611
17 Dmitri V Louzguine, Akihisa Inoue. *Journal of Non-Crystalline Solids*[J], 2004, 337: 161
18 Qiang J B, Zhang W, Inoue A. *Materials Transactions*[J], 2007,48 (9): 2385
19 Zhang T, Inoue A. *Materials Science and Engineering A*[J], 2007, 304(3): 771
20 Zhang Tao, Inoue Akihisa. *Materials Transactions*[J], 2002, 43(2): 708
21 Louzguine-Luzgin Dmitri V, Shimada Takeyuki, Inoue Akihisa. *Intermetallics*[J], 2005, 13: 1166
22 Zeng Yuqiao, Qin Chunling, Nishiyama Nobuyuki *et al*. *Journal of Alloys and Compounds*[J], 2010, 489: 80
23 Xu Donghua, Duan Gang, William L *et al*. *Acta Materialia*[J], 2004, 52: 3493
24 Shen Baolong, Inoue Akihisa. *Materials Transactions*[J], 2003, 44(7) : 1425
25 Shen Baolong, Chang Chuntao, Inoue Akihisa. *Applied Physics Letters*[J], 2006, 88: 201 903
26 Inoue A, Zhang T, Masumoto T. *Materials Transactions*[J], 1989, 30: 965
27 Takeuchi Akira, Inoue Akihisa. *Materials Transactions*[J], 2005, 46(12): 2817
28 Movahedi B, Enayati M H, Wong C C. *Journal of Thermal Spray Technology*[J], 2010, 19(5): 1093
29 Ouyang Hongwu, Chen Xin, Yu Wentao *et al*. *Rare Metal Materials and Engineering*[J], 2006, 35(5): 866 (in Chinese)
30 Trivedi R, Kurz W. *Acta Metallurgica*[J], 1986, 34(5): 823
31 Ni H S, Liu X H, Chang X C *et al*. *Journal of Alloys and Compounds*[J], 2009, 467: 163
32 Lu Z P, Liu C T. *Acta Materialia*[J], 2002, 50: 3501
33 Long Z L, Xie G Q, Wei H Q *et al*. *Materials Science and Engineering A*[J], 2009, 509: 23

一种新型经济高效非晶涂层的制备与性能

商俊超[1]，梁秀兵[2]，陈永雄[2]，徐滨士[1]，曹　维[3]
(1. 陆军装甲兵学院 装备再制造技术国防科技重点实验室，北京 100072)
(2. 军事科学院 国防科技创新研究院，北京 100070)
(3. 中国人民解放军 63963 部队，北京 100072)

摘　要：以自制的气雾化合金粉末取代非晶粉末，利用火焰喷涂技术制备了 NiFeBSiNb 非晶纳米晶涂层。分别对粉末和涂层的微观结构和热力学性能进行了表征。结果表明，自制的合金粉末球形度较好，大多为球形或椭球形；主要为晶体结构，由 $Nb_2Ni_{21}B_6$ 晶体相和 $(Ni,Fe)_{23}B_6$ 固溶体组成。而经过火焰喷涂制备的涂层，形成了非晶相和纳米晶相。通过公式计算此合金体系粉末和涂层形成非晶相的临界冷却速率分别为 6.01×10^5 和 4.56×10^3 K/s，解释了在粉末制备过程中较难形成非晶相而喷涂过程中形成非晶结构比较容易的原因。对涂层的摩擦磨损性能进行了测试，涂层摩擦系数仅为 0.17，具有优异的耐磨性能。

关键词：非晶涂层；合金粉末；火焰喷涂；摩擦磨损

作者简介：商俊超，男，1988 年生，博士生，陆军装甲兵学院装备再制造技术国防科技重点实验室，北京 100072，电话：010-66717351，E-mail: shangjc2011@163.com